The Astrophysical Journal, 778:116 (14pp), 2013 December 1 doi:10.1088/0004-637X/778/2/116

REAPPEARANCE OF McNEIL'S NEBULA (V1647 ORIONIS) AND ITS OUTBURST ENVIRONMENT

J. P. Ninan[1], D. K. Ojha[1], B. C. Bhatt[2], S. K. Ghosh[3], V. Mohan[4], K. K. Mallick[1], M. Tamura[5], and Th. Henning[6]

[1] Department of Astronomy and Astrophysics, Tata Institute of Fundamental Research, Homi Bhabha Road, Colaba, Mumbai 400 005, India; ninan@tifr.res.in
[2] Indian Institute of Astrophysics, Koramangala, Bangalore 560 034, India
[3] National Centre for Radio Astrophysics, Tata Institute of Fundamental Research, Pune 411 007, India
[4] Inter-University Centre for Astronomy and Astrophysics, Pune 411 007, India
[5] National Astronomical Observatory of Japan, Mitaka, Tokyo 181-8588, Japan
[6] Max-Planck-Institute for Astronomy, Königstuhl 17, D-69117 Heidelberg, Germany
Received 2013 June 4; accepted 2013 September 16; published 2013 November 11

ABSTRACT

We present a detailed study of McNeil's nebula (V1647 Ori) in its ongoing outburst phase starting from 2008 September to 2013 March. Our 124 nights of photometric observations were carried out in optical *V*, *R*, *I*, and near-infrared *J*, *H*, *K* bands, and 59 nights of medium-resolution spectroscopic observations were done in the 5200–9000 Å wavelength range. All observations were carried out with the 2 m Himalayan Chandra Telescope and 2 m IUCAA Girawali Telescope. Our observations show that over the past four and a half years, V1647 Ori and region C near the Herbig–Haro object HH 22A have been undergoing a slow dimming at a rate of ∼0.04 mag yr^{-1} and ∼0.05 mag yr^{-1}, respectively, in *R* band, which is six times slower than the rate during a similar stage of V1647 Ori in the 2003 outburst. We detected change in flux distribution over the reflection nebula, implying changes in circumstellar matter distribution between the 2003 and 2008 outbursts. Apart from steady wind of velocity ∼350 km s^{-1}, we detected two episodic magnetic reconnection driven winds. Forbidden [O I] λ6300 and [Fe II] λ7155 lines were also detected, implying shock regions probably from jets. We tried to explain the outburst timescales of V1647 Ori using the standard models of the FUors kind of outburst and found that pure thermal instability models like Bell and Lin cannot explain the variations in timescales. In the framework of various instability models we conclude that one possible reason for the sudden ending of the 2003 outburst in 2005 November was a low-density region or gap in the inner region (∼1 AU) of the disk.

Key words: accretion, accretion disks – circumstellar matter – ISM: individual objects (McNeil's nebula) – stars: individual (V1647 Ori) – stars: pre-main sequence

Online-only material: color figures, extended figure, figure set, machine-readable tables

1. INTRODUCTION

When low-mass stars like our Sun are born, they slowly accrete gas from the collapsing cloud through an accretion disk. Collimated outflows are also typically seen in most of these objects. The discontinuous knots seen in outflows from these objects, and the mismatch of accretion rate between envelope to disk and disk to star (known as the "luminosity problem") in young stellar objects (YSOs), all hint to an episodic nature of accretion instead of an ideal steady inflow (Kenyon et al. 1990; Evans et al. 2009; Ioannidis & Froebrich 2012). The other important feature seen in these objects is the outburst. Rare outbursts that we see among these YSOs are found to be correlated with an order-of-magnitude increase in mass infall rate, and they could be the episodic accretion events required to explain the outflow discontinuities and the "luminosity problem." These outbursts are empirically classified as FUors (decades-long outbursts with 4–5 mag change in optical) and EXors (few months–years long outbursts with 2–3 mag change in optical; Herbig 1977; Hartmann 1998; Hartmann & Kenyon 1996). Due to the short timescales of outbursts in comparison to the millions-of-years timescale of star formation, these events are extremely rare, and only less than a dozen confirmed FUor outbursts have been detected so far. From their frequency of outburst it is estimated that every low-mass YSO should go through these outbursts at least 50 times in its protostellar phase (Scholz et al. 2013). Regarding the discontinuous knots seen in outflows, it should be noted that the timescales between discontinuities were estimated to be of the order of 10^3 yr by Ioannidis & Froebrich (2012), and the timescales between FUor outbursts in a single star were estimated to be of the order of 10^4 yr by Scholz et al. (2013). So the discontinuities could be due to some other shorter timescale variations in accretion rate rather than classical FUors. But as Scholz et al. (2013) pointed out, we do not have a good estimate of FUors' timescales in the early Class I stage. Hence, we cannot rule out the possibility that discontinuities in outflows are created during FUors events.

One such object that was extensively studied recently in literature is V1647 Ori (V1647 Orionis), 400 pc away in the L1630 dark cloud of Orion. It underwent a sudden outburst of ∼5 mag in optical in 2003 (McNeil 2004; Briceño et al. 2004) and illuminated a reflection nebula, now named as McNeil's nebula after its discoverer Jay McNeil. Reipurth & Aspin (2004) reported 3 mag increase in near-infrared (NIR) and Andrews et al. (2004) reported 25 times increase in 12 μm flux and no flux change in submillimeter of V1647 Ori during the outburst. Kastner et al. (2004) reported a 50 times increase in X-ray flux of V1647 Ori during the outburst and noted that the derived temperature of the plasma is too high for accretion alone to explain, hinting that magnetic reconnection events might be heating up the plasma. Based on the upper limit on radio continuum emission from McNeil's nebula at 1272 MHz from the Giant Metrewave Radio Telescope, India, Vig et al. (2006) constrained the extent of the H II region corresponding to a

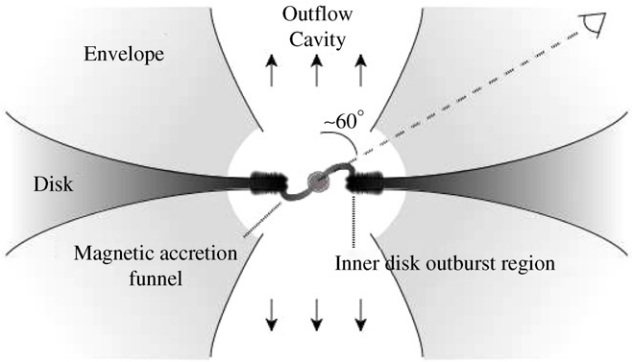

Figure 1. Cross section of V1647 Ori surroundings we know so far and the line-of-sight angle to the disk. Image is not drawn to scale.

temperature $\gtrsim$2500 K to be $\lesssim$26 AU. Spectroscopic studies showed strong Hα and Ca II IR triplet lines in emission (Briceño et al. 2004; Ojha et al. 2006). In the NIR region, strong CO bandheads (2.29 μm) and a Brγ line (2.16 μm; implying strong accretion) were detected in emission (Reipurth & Aspin 2004; Vacca et al. 2004). The strong P Cygni profile in Hα emission indicated wind velocity ranging from 600 to 300 km s^{-1} (Ojha et al. 2006; Vacca et al. 2004). Ábrahám et al. (2006) carried out AU-scale observations using the Very Large Telescope Interferometer/Mid-Infrared interferometric Instrument (VLTI/MIDI). By fitting both spectral energy distribution (SED) and visibility values, they deduced a moderately flaring disk with temperature profile $T \sim r^{-0.53}$ (T(1 AU) = 680 K) and mass $\sim$ 0.05 $M_\odot$, with inner radius of 7 $R_\odot$ (0.03 AU) and outer radius of 100 AU. This temperature profile is shallower than the $T \sim r^{-0.75}$ canonical model (Pringle 1981). They also reported that the mid-infrared emitting region at 10 μm has a size of $\sim$7 AU. Rettig et al. (2005) used the CO lines in infrared (IR) to measure the temperature of the inner accretion disk region, which was estimated to be $T \approx 2500$ K.

Ojha et al. (2006) and Kóspál et al. (2005) reported a sudden dimming and termination of the 2003 outburst in 2005 November. Thus, the 2003 outburst lasted for a total of $\sim$2 yr, and V1647 Ori returned to its pre-outburst phase in early 2006. Acosta-Pulido et al. (2007) estimated the inclination angle of the disk to be 61° and also estimated the accretion rate to be $5 \times 10^{-6}\,M_\odot$ yr^{-1} during outburst and $5 \times 10^{-7}\,M_\odot$ yr^{-1} in the 2006 quiescent state. Aspin et al. (2006) reported that $\sim$37 yr prior to the 2003 outburst, i.e., in 1966, V1647 Ori had undergone a similar magnitude of outburst, lasting somewhere between 5 and 20 months.

Contrary to expected decades-long quiescence, V1647 Ori underwent a second outburst in 2008 just after spending 2 yr in a quiescent state (Aspin et al. 2009). It brightened up to the same magnitude and had almost identical spectral features in optical and NIR as the first outburst. One striking difference was that the strong CO bandhead emission at 2.29 μm was absent in the second outburst (Aspin 2011). The X-ray flux with plasma temperature of 2–6 keV during both outbursts was postulated to be due to magnetic reconnection events in the disk–star magnetic field interaction (Teets et al. 2011, and references therein). Hamaguchi et al. (2012) normalized and combined both outbursts' data in X-ray and detected 1 day periodicity in the light curve, which they modeled with two accretion hot spots on the top and bottom hemispheres of the star rotating with 1 day period and inclination of 68°. Figure 1 shows the overall cross-section picture of the surroundings of V1647 Ori we know so far.

V1647 Ori provides a unique opportunity to understand the physical processes undergone in the FUors or EXors kind of outbursts. The short-timescale behaviors of this object make it possible for us to make a detailed study of the object. In the literature there exists mainly three kinds of models for explaining the outburst phenomena (see Section 4). The differences between these models are all in the inner region of the disk (<1 AU), and optical and NIR are the right wavelength regimes to probe this region of the disk. Detailed understanding of V1647 Ori will thus provide us a laboratory to check our understanding of various instabilities like thermal, gravitational, and magnetorotational in proto-planetary disks around young low-mass stars.

We have carried out continuous observations for more than four and a half years (2008–2013) of V1647 Ori in optical and NIR wavelengths for detailed study of its dynamics during outburst and post-outburst stages of the second outburst. These data combined with previous outbursts' provide us more insight on the nature of outbursts and also constrain the existing physical models. In this paper, we present the results of our long-term optical and NIR photometric and spectroscopic observations of the outburst source and associated McNeil's nebula. In Section 2 we describe the observational details and the data reduction procedures. In Section 3 we present our new findings and results from observations. In Section 4 we analyze the ability of each existing physical model to explain V1647 Ori's outburst history. Finally, in Section 5 we summarize our main results.

2. OBSERVATIONS AND DATA REDUCTION

2.1. Optical Photometry

Our long-term optical observations span from 2008 September 14 to 2013 March 11 and were carried out with the 2 m Himalayan Chandra Telescope (HCT) at the Indian Astronomical Observatory, Hanle (Ladakh), India, and with the 2 m Inter-University Centre for Astronomy and Astrophysics (IUCAA) Girawali Telescope at the IUCAA Girawali Observatory (IGO), Girawali (Pune), India. At HCT, for photometry the central 2K × 2K section of the Himalaya Faint Object Spectrograph & Camera (HFOSC) CCD, which has a pixel scale of 0.″296, was used, giving us a field of view (FOV) of $\sim$10 × 10 arcmin^2. At IGO, the 2K × 2K IUCAA Faint Object Spectrograph & Camera (IFOSC) CCD was used, which also has a similar pixel scale of 0.″3, giving us an FOV of $\sim$10 × 10 arcmin^2. Further details of the instruments and telescopes are available at http://www.iiap.res.in/iao/hfosc.html and http://www.iucaa.ernet.in/~itp/igoweb/igo_tele_and_inst.htm. Out of our total observation of 110 nights, 84 nights were observed from HCT and 26 nights from IGO.

V1647 Ori's field, $(\alpha, \delta)_{2000}$ = ($05^h46^m13\overset{s}{.}135$, $-00°06'04\overset{''}{.}82$), was observed in standard VRI Bessel filters. Nearby Landolt's standard star fields (Landolt 1992) were also observed for magnitude calibration and for solving color transformation equation coefficients of each night. For nights that do not have standard star observations, we identified six stars in the object's frame whose magnitudes remain constant throughout. Four of them were used as secondary standards (see Figure 2), and the other two were used to check consistency and error. Apart from object frames, bias and sky flats were also taken on each night for the basic data reduction. For fringe removal in IGO I-band images, blank sky frames were also taken. The log

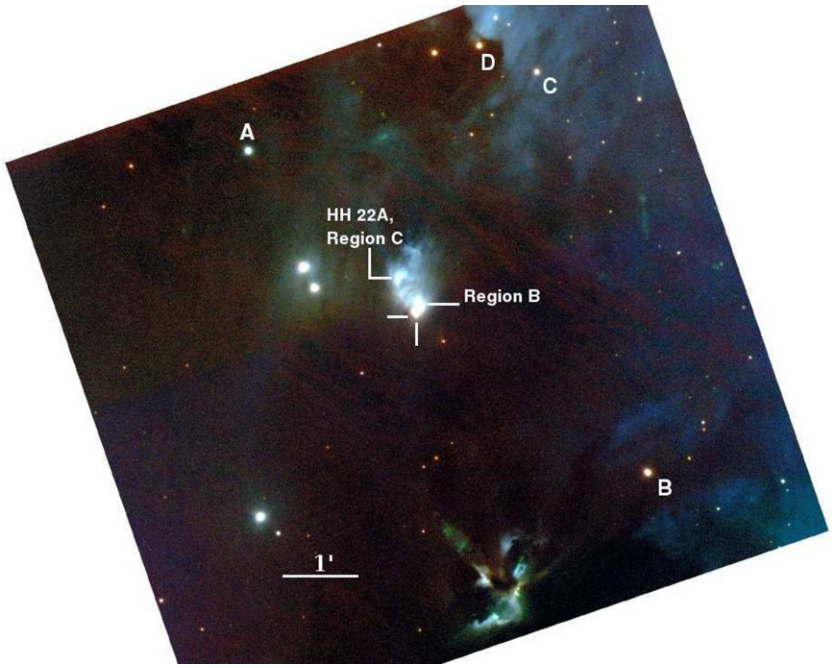

Figure 2. Color-composite image of McNeil's nebula (V1647 Ori) region taken from IGO (*V*: blue; *R*: green; *I*: red) on 2010 February 13. The FOV is ∼10 × 10 arcmin^2. North is up and east is to the left-hand side. Stars marked as A, B, C, and D are the secondary standard stars used for magnitude calibration. The location of V1647 Ori is marked at the center by two perpendicular lines. Region C, overlapping Herbig–Haro object HH 22A, is marked together. A knot in the southwestern section (region B) of the nebula is also marked. At 400 pc distance, the scale 1′ corresponds to 24,000 AU.

(A color version of this figure is available in the online journal.)

Table 1
Observation Log of the Photometric and Spectroscopic Observations

Date (UT)	JD	FWHM†	Filter(s)/Grism(s)	Exposure Time (s)
2008 Sep 14	2,454,724	1.″9	$V, R, I, gr8$	300, 480, 240, 2400
2008 Sep 15	2,454,724	1.″6	$gr8$	2400
2008 Sep 16	2,454,726	1.″5	V, R, I	600, 720, 240
2008 Sep 28	2,454,738	1.″1	V, R, I	240, 240, 180
2008 Oct 1	2,454,741	1.″2	V, R, I	120, 120, 90
2008 Oct 2	2,454,742	1.″2	$V, R, I, gr7$	240, 240, 180, 2400
2008 Oct 3	2,454,743	1.″5	$gr8$	2400

Notes.
† Measured average FWHM. This is a measure of the seeing.
†† Observed from IGO; all other nights are from HCT.

(This table is available in its entirety in a machine-readable form in the online journal. A portion is shown here for guidance regarding its form and content.)

of photometric observations is given in Table 1. Only a portion of the table is provided here. The complete table is available in machine-readable form in the online journal.

Blank sky images in *I* band were used to create fringe templates by the MKFRINGECOR task in IRAF,[7] which were later used to subtract the fringes that appeared in *I*-band images taken from IGO. Data reduction was done with the semi-automatic pipeline written in PyRAF[8] and IRAF command language scripts. Standard photometric data reduction steps like bias subtraction and median flat-fielding were done for all the nights. Point-spread function (PSF) photometry (using PSF and ALLSTAR tasks in the DAOPHOT package of IRAF) on V1647 Ori was not able to fully remove the nebular contamination. We found a strong correlation between fluctuation in magnitude of V1647 Ori and fluctuation in atmospheric seeing condition. This is because the contamination of flux from the nebula into V1647 Ori's aperture was a function of atmospheric seeing. So we generated a set of images by convolving each frame with two-dimensional Gaussian kernel of different standard deviation (using the IMFILTER.GAUSS task in IRAF) for simulating different atmospheric seeing conditions. We then recalculated the magnitudes by DAOPHOT, PSF, and ALLSTAR algorithms of IRAF for various atmospheric seeing conditions. The differential magnitudes obtained from each frame's set were interpolated to obtain magnitude at an atmospheric seeing of 1.″18, which was taken to be the seeing to be interpolated to for all nights, and it was chosen to minimize interpolation error. This method reduced our error bars in magnitude by a factor of two. Apart from the Gaussian convolution step, the PSF photometry steps were all the same as in Ojha et al. (2006).

Magnitudes of the whole nebula and other objects in the nebula like region C (near HH 22A) and region B defined by Briceño et al. (2004) in their Figure 2 (also see Figure 2) were measured by simple aperture photometry with an aperture radius of 80 arcsec for nebula and 12 arcsec for regions C and B. For obtaining the flux, the aperture of objects like regions C and B was centered at the objects themselves.

2.2. Optical Spectroscopy

Our long-term spectroscopic observations also span the same duration as that of photometric observations (2008 September to 2013 March) using both 2 m HCT and 2 m IGO. The full 2K × 4K section of the HFOSC CCD spectrograph was used in HCT observations, and the 2K × 2K IFOSC CCD spectrograph was used for IGO observations. Spectroscopic observations

[7] IRAF is distributed by the National Optical Astronomy Observatory, which is operated by the Association of Universities for Research in Astronomy, Inc., under cooperative agreement with the National Science Foundation.
[8] PyRAF and PyFITS are products of the Space Telescope Science Institute, which is operated by AURA for NASA.

were carried out on 35 nights from HCT and 24 nights from IGO, thus totaling 59 nights of V1647 Ori's spectroscopic observations. The log of spectroscopic observations is listed in Table 1. Only a portion of the table is provided here. The complete table is available in machine-readable form in the online command language. In order to detect the prominent Hα λ6563 and Ca II IR triplet lines (λ8498, λ8542, λ8662), we observed in the effective wavelength range of 5200–9000 Å using grism 8 (center wavelength 7200 Å) and grism 7 (center wavelength 5300 Å). The spectral resolution obtained for grism 8 and 7 with 150 μm slit at IGO and 167 μm slit at HCT was ~7 Å. Nebulosity contamination in the spectrum of V1647 Ori was minimized by keeping the slit in east-west orientation. Standard IRAF tasks like APALL and APSUM were used for spectral reduction. Wavelength calibration was carried out using the FeNe, FeAr, and HeCu lamps. For final measurement of equivalent width the extracted one-dimensional spectra were normalized with respect to continuum. For spectroscopic data reduction of HCT and IGO data, a semi-automated pipeline written in PyRAF was used.

2.3. Near-Infrared Photometry

Along with optical monitoring we also carried out photometric monitoring in *JHK* bands using the HCT NIR camera (NIRCAM) and TIFR NIR Imaging Camera-II (TIRCAM2). NIRCAM has a 512 × 512 Mercury Cadmium Telluride (HgCdTe) array, with a pixel size of 18 μm, which gives an FOV of 3.6 × 3.6 arcmin^2 with HCT. Filters used for observation were J (λ_{center} = 1.28 μm, $\Delta\lambda$ = 0.28 μm), H (λ_{center} = 1.66 μm, $\Delta\lambda$ = 0.33 μm), and K (λ_{center} = 2.22 μm, $\Delta\lambda$ = 0.38 μm). Further details of the instrument are available at http://www.iiap.res.in/iao/nir.html. TIRCAM2 has a 512 × 512 Indium Antimonide (InSb) array with a pixel size of 27 μm. We observed McNeil's nebula during the engineering run of TIRCAM2 at 2 m IGO and the 1.2 m Physical Research Laboratory Mount Abu telescope. Filters used for observation were J (λ_{center} = 1.20 μm, $\Delta\lambda$ = 0.36 μm), H (λ_{center} = 1.66 μm, $\Delta\lambda$ = 0.30 μm), and K (λ_{center} = 2.19 μm, $\Delta\lambda$ = 0.40 μm). Further details of the instrument are available in Naik et al. (2012). We have a total of 14 nights of NIR photometric observations, with the first set of data taken during the quiescent phase in 2007, i.e., before the 2008 outburst. Observations of V1647 Ori were carried out by taking several sets of exposures; each set contains exposure with the telescope pointing at five different dithered positions. The master sky frame for sky subtraction was generated by median combining all the dithered object frames. Data reduction and final photometry were done using standard IRAF aperture photometric tasks. To be consistent with magnitude estimates by Ojha et al. (2006), for flux calibration we used an aperture of ~7 arcsec, and for background sky estimation we used an annulus with an inner radius of ~50″ and width ~5″. For instrumental to apparent magnitude calibration, we observed standard stars around AS13, AS9, and HD 225023 fields (Hunt et al. 1998) on the same night with similar airmass as V1647 Ori observations. On 2011 December 6, standard stars were not observed; hence, we used the magnitude measured on other nights of the nearby star (2MASS J05461162−0006279) for photometric calibration.

3. RESULTS AND DISCUSSION

3.1. Photometric Results

Figure 2 shows the three-color composite image (V: blue; R: green; I: red) of the McNeil's nebula field (FOV ~ 10 × 10 arcmin^2) obtained from IGO on 2010 February 13. Secondary standard stars used for flux calibration are marked as A, B, C, and D. The outburst source V1647 Ori, illuminating the nebula, is marked at the center. Region C, possibly unrelated to Herbig–Haro object HH 22A, which is illuminated by V1647 Ori, is also marked. V1647 Ori had already reached its peak outburst phase before our first optical observation in 2008 September. Its light curve steadily continued in peak outburst flux ("high plateau") phase even until our last observation taken in 2013 March. However, our long-term continuous monitoring from 2008 September 14 to 2013 March 11 shows a slow but steady linear declining trend in the brightness of the source and nebula (Ninan et al. 2012). The linear slopes and the error in estimates of slopes were obtained by simple linear regression by ordinary least-squares fitting. V, R, and I magnitudes of V1647 Ori and of region C, which is illuminated by V1647 Ori from its face-on angle of the disk, are listed in Table 2. Only a portion of the table is provided here. The complete table is available in machine-readable form in the online journal. Light curves of V1647 Ori in I and R bands clearly show a steady dimming (see Figure 3). During the past four and a half years of its second outburst, the brightness in I and R bands has decreased by ~0.2 mag. The rate of decline in magnitude of V1647 Ori is 0.036 ± 0.007 mag yr^{-1} in I band and 0.038 ± 0.007 mag yr^{-1} in R band. We do not see any statistically significant decline in V-band magnitude of V1647 Ori. This could be due to the higher fraction of contamination of the nebula over V1647 Ori's aperture and slightly higher error in magnitudes due to faintness of the source in V band. These flux changes are along our direct line of sight at an angle of ~30° to the plane of the disk (Acosta-Pulido et al. 2007). However, the flux measured along the cavity in perpendicular direction to the disk, which is reflected from region C, shows a dimming trend of 0.059 ± 0.005 mag yr^{-1} in I band, 0.051 ± 0.005 mag yr^{-1} in R band, and 0.060 ± 0.005 mag yr^{-1} in V band (see Figure 4). Hence, region C seems to be dimming faster than V1647 Ori. This could be either due to material inflow into cavity between region C and V1647 Ori as the outburst is progressing or due to a change in extinction along the cavity induced by slow dimming of V1647 Ori's brightness. During the first outburst in 2003, the linear dimming rate during the plateau stage was 0.24 mag yr^{-1} in R band (Fedele et al. 2007), which was ~6.3 times faster in magnitude scale than the present dimming rate in the second outburst. Just like in other T Tauri stars, we also see a lot of short-timescale

Table 2
Optical V R I Photometry of V1647 Ori and Region C

Julian Date	V1647 Ori			Region C		
	V	R	I	V	R	I
2,454,724	19.08	17.06	14.98	15.59	14.99	14.36
2,454,726	19.11	17.11	15.04	15.57	14.98	14.36
2,454,738	19.00	17.04	14.99	15.59	15.06	14.36
2,454,741	19.04	17.05	15.02	15.59	14.98	14.33
2,454,742	19.09	17.09	15.04	15.55	15.02	14.39
2,454,745	19.12	···	15.02	15.60	···	14.30
2,454,751	19.26	17.08	15.02	15.50	15.02	14.20

Notes. Estimated error in magnitude of V1647 Ori is ⩽±0.05 for V and ⩽±0.02 for R and I. Estimated error in magnitude of region C is ⩽±0.02 for V, R, and I.
†† Observed from IGO; all other nights are from HCT.

(This table is available in its entirety in a machine-readable form in the online journal. A portion is shown here for guidance regarding its form and content.)

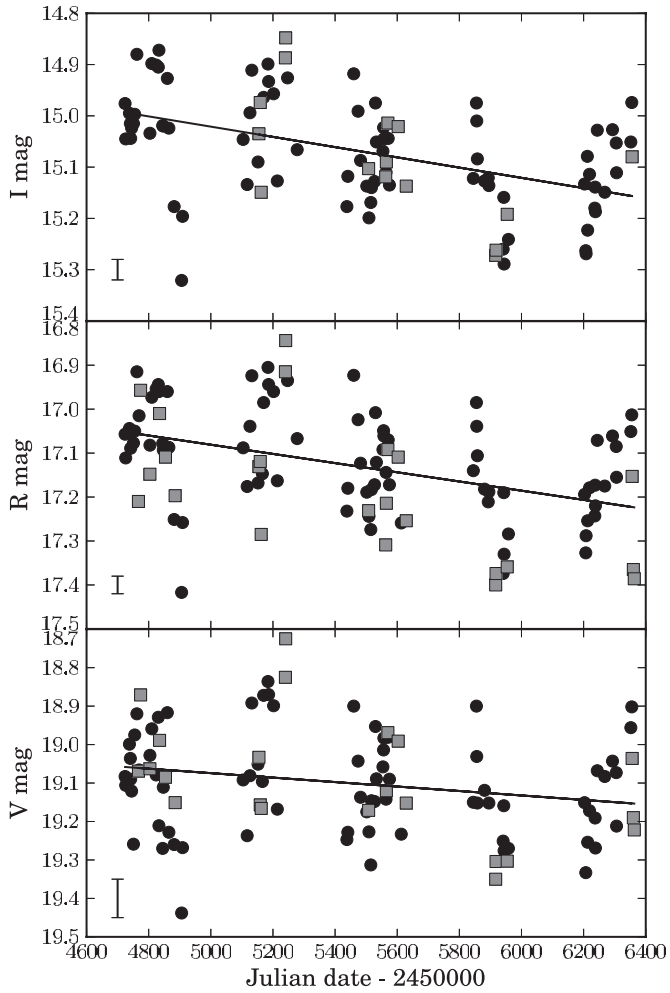

Figure 3. Magnitude variation of V1647 Ori in the *I, R*, and *V* band from 2008 September to 2013 March. The typical photometric error bar is given in the left bottom corner. The filled circles are from HCT, and filled squares are from IGO measurements. The rate of dimming in *I, R*, and *V* bands is 0.036 ± 0.007 mag yr^{-1}, 0.038 ± 0.007 mag yr^{-1}, and 0.021 ± 0.009 mag yr^{-1}, respectively.

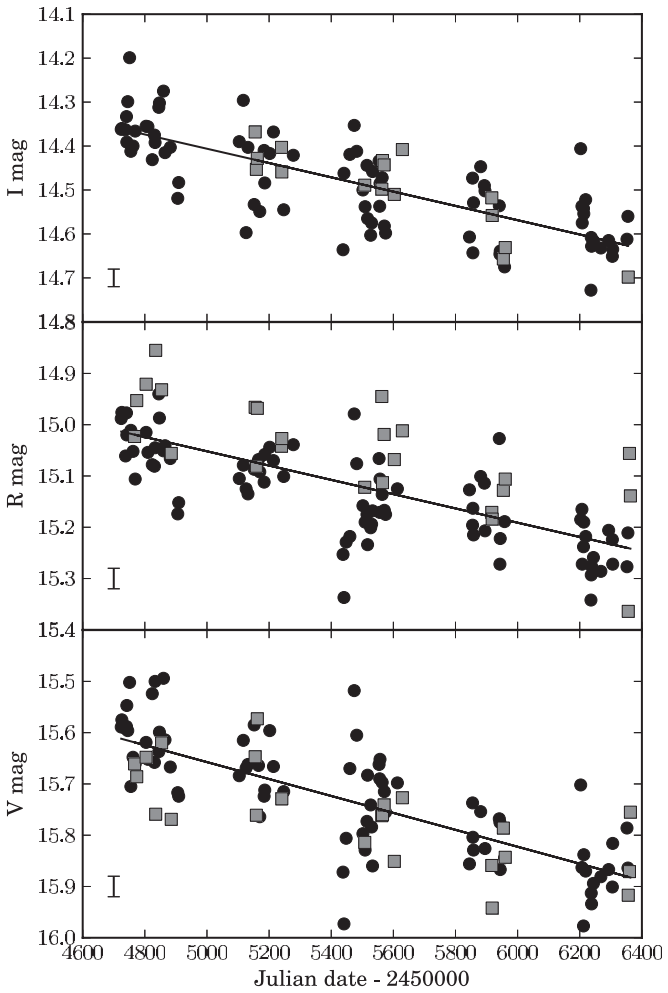

Figure 4. Magnitude variation of region C, illuminated by V1647 Ori, in the *I, R*, and *V* band from 2008 September to 2013 March. The typical photometric error bar is given in the left bottom corner. The filled circles are from HCT, and filled squares are from IGO measurements. The rate of dimming in *I, R*, and *V* bands is 0.059 ± 0.005 mag yr^{-1}, 0.051 ± 0.005 mag yr^{-1}, and 0.060 ± 0.005 mag yr^{-1}, respectively.

random variations in the source magnitude (peak-to-peak $\Delta V \simeq 0.35$ mag, $\Delta R \simeq 0.30$ mag, and $\Delta I \simeq 0.20$ mag), which could be due to density fluctuations in the infalling gas on to the star.

Our light curve of V1647 Ori does not show any 56 day periodicity, which was reported by Acosta-Pulido et al. (2007) during the first 2003 outburst. Based on the correlated reddening of flux during the minima of light curve, they proposed that periodicity was due to occultation of a dense clump in the accretion disk at a distance of 0.25 AU from the star. The peak-to-peak amplitude in *I* band was ∼0.3 mag in 2003. We have not detected this variability in the 2008 outburst, which implies that the dense clump might have gotten dissipated between the 2003 and 2008 outburst events. Our Lomb–Scargle periodogram analysis of magnitudes did not show any other statistically significant periodicity.

The optical magnitudes during the second outburst are almost similar to that of the first outburst in 2003. In fact, the first known outburst of V1647 Ori in 1966 (∼38 yr prior to 2003), reported by Aspin et al. (2006), also had similar magnitude to the present one; however, all three outbursts have different timescales. Implications of this fact on outburst model will be discussed in Section 4.

Table 3
NIR *JHK* Photometry of V1647 Ori

Date (UT)	*J*	*H*	*K*	Instrument
2007 Oct 28	14.12	11.43	9.36	NIRCAM
2008 Oct 19	10.64	9.01	7.63	NIRCAM
2009 Jan 12	10.59	8.76	7.62	NIRCAM
2009 Feb 12	11.04	9.01	7.51	NIRCAM
2009 Feb 18	10.87	9.16	7.68	NIRCAM
2009 Oct 23	10.71	8.89	7.40	NIRCAM
2009 Oct 24	10.71	8.88	7.44	NIRCAM
2010 Feb 20	10.75	8.96	7.43	NIRCAM
2010 Mar 23	10.73	9.14	...	NIRCAM
2011 Nov 18	10.75	8.90	7.58	NIRCAM
2011 Dec 3	10.94	9.28	7.41	TIRCAM2
2011 Dec 4	10.97	9.19	7.42	TIRCAM2
2011 Dec 6	10.84	9.10	7.47	TIRCAM2
2012 Nov 7	10.73	9.01	7.46	NIRCAM

Note. Estimated error in magnitude is $\leqslant \pm 0.1$ (*K*) and $\leqslant \pm 0.05$ (*H* and *J*).

Our NIR *J*, *H*, and *K* magnitudes are listed in Table 3. Similar to optical light curve, there is a faint dimming trend in NIR also. Venkata Raman et al. (2013), with more NIR data points,

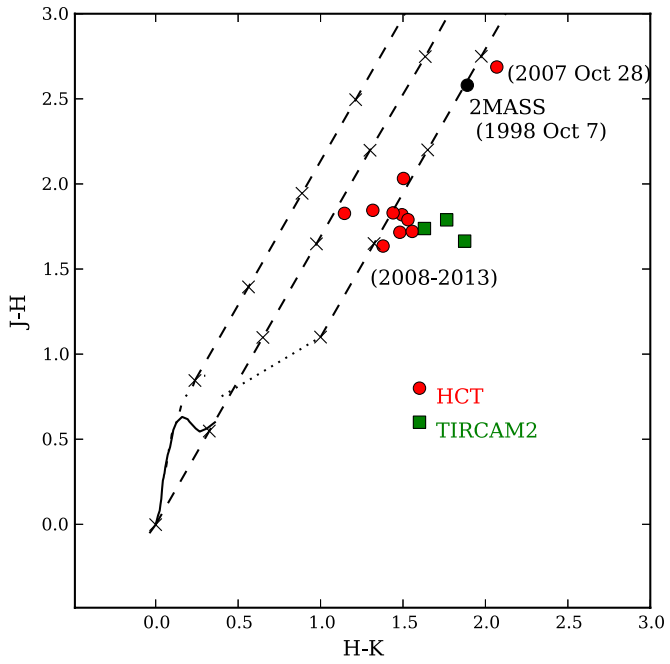

Figure 5. Movement of the position of V1647 Ori in the $J - H/H - K$ CC diagram from the quiescent phase in 2007 to the second outburst phase. The solid curve shows the locus of field dwarfs, and the dash–dotted curve shows the locus of giants (Bessell & Brett 1988). The dotted line represents the locus of CTT stars (Meyer et al. 1997). The diagonal straight dashed lines show the reddening vectors (Rieke & Lebofsky 1985), with crosses denoting an A_V difference of 5 mag.

(A color version of this figure is available in the online journal.)

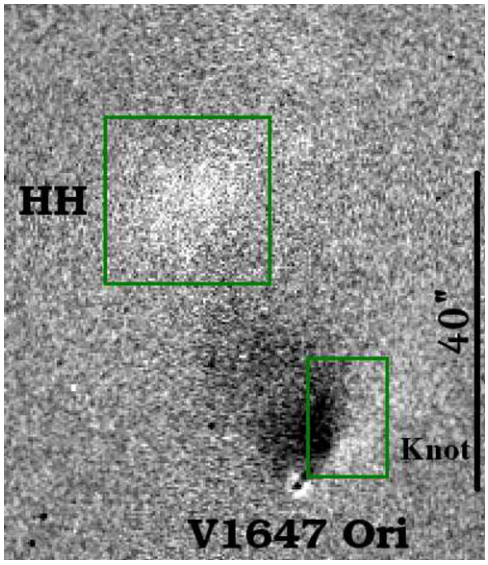

Figure 6. HCT *R*-band image of 2011 minus 2004, after normalizing with respect to the brightness of V1647 Ori. The images were chosen from the nights with the same atmospheric seeing and aligned using other field stars in the FOV. The bright portions show the regions that were relatively brighter in 2011, and dark portions show the regions that were relatively brighter in 2004. For example, region C shown in the upper box is brighter in 2011. Also note the change in illumination of southwestern knot region B marked by the lower box in the nebula. North is up and east is to the left-hand side.

(A color version of this figure is available in the online journal.)

estimated the fading rate in *J* band to be 0.08 ± 0.02 mag yr^{-1}. The $J - H/H - K$ color–color (CC) diagram (Figure 5) shows the movement of V1647 Ori from the 2007 data point taken in quiescent phase to outburst state. It is similar to what was seen in the 2003 outburst. From the quiescent phase position in the CC diagram, V1647 Ori has moved toward the classical T Tauri (CTT) locus along the reddening vector and currently occupies the same position as in the 2003 outburst. The position of V1647 Ori in the CC diagram is consistent with a similar CC diagram published by Venkata Raman et al. (2013). This implies that the decrease in line-of-sight extinction during the outburst is the same as that seen during the 2003 outburst. Since our line of sight is through the envelope, it must be likely due to a reversible mechanism like dust sublimation in the inner region of the envelope during each outburst (Acosta-Pulido et al. 2007; Mosoni et al. 2013; Aspin et al. 2009). Since the star is deeply embedded, we have reflections and dust emission effects also affecting the position of V1647 Ori in the CC diagram. So the extinction estimated from the CC diagram is not very reliable. Otherwise, we can see that the second outburst has cleared out circumstellar matter of $\delta A_V \sim 6 \pm 2$ mag. This is also consistent with the estimate of extinction change during first outburst by Mosoni et al. (2013), $\delta A_V \sim 4.5$ mag (see also Aspin et al. 2008).

3.2. Morphological Results

Between the 2003 and 2008 outbursts, McNeil's nebula does not have any significant morphological changes; however, the intensity distribution of the nebula has changed between the outbursts. Figure 6 shows the difference in *R*-band flux along the nebula between 2011 and 2004. Images of similar atmospheric conditions were taken and scaled to match the brightness of V1647 Ori before subtracting the 2004 image from that of 2011. Brighter shade implies that the region is brighter in 2011 than 2004. We can see that region C is brighter in the second outburst than it was in 2004. This could be due to dust clearing up between the last two outbursts along the cavity seen in NIR in the region C direction (Ojha et al. 2005). Our photometric results show that region C is dimming faster than V1647 Ori, and one of the explanations for that could be material inflow into the cavity during the outburst. However, region C is relatively brighter in the 2008 outburst than in 2004 for the same brightness of V1647 Ori. This implies that the matter inflow to the cavity was not occurring during the quiescent phase between 2006 and 2008. This is also based on the implicit assumption that the extinction along the line-of-sight direction to V1647 Ori is the same between the 2003 and 2008 outbursts. The other significant change is in illumination of the southwestern knot (region B) of the nebula; its illumination seems to have shifted slightly toward west. These illumination changes in the nebula imply a structural change in the circumstellar matter above the disk and cavity. A similar pattern and conclusion were also reported between the 1966, 2003, and 2008 outbursts by Aspin et al. (2006, 2009). Similar analysis of image pairs taken between 2008 and 2012 did not show any significant morphological changes. Our image pairs had a seeing of 1.″6. Hence, to check whether any change in illumination of nebula is occurring during the present outburst, we need images with seeing less than 1.″6.

3.3. Spectroscopic Results

V1647 Ori optical spectra show strong Hα (6563 Å) emission and a Ca II IR triplet at 8498, 8542 and 8662 Å in emission. Other weak lines seen are Na D (5890+5896 Å) and O I (7773 Å) in absorption and [O I] (6300 Å), O I (8446 Å), [Fe II] (7155 Å), and Fe I (8388, 8514 Å) in emission (see Figure 7). The equivalent

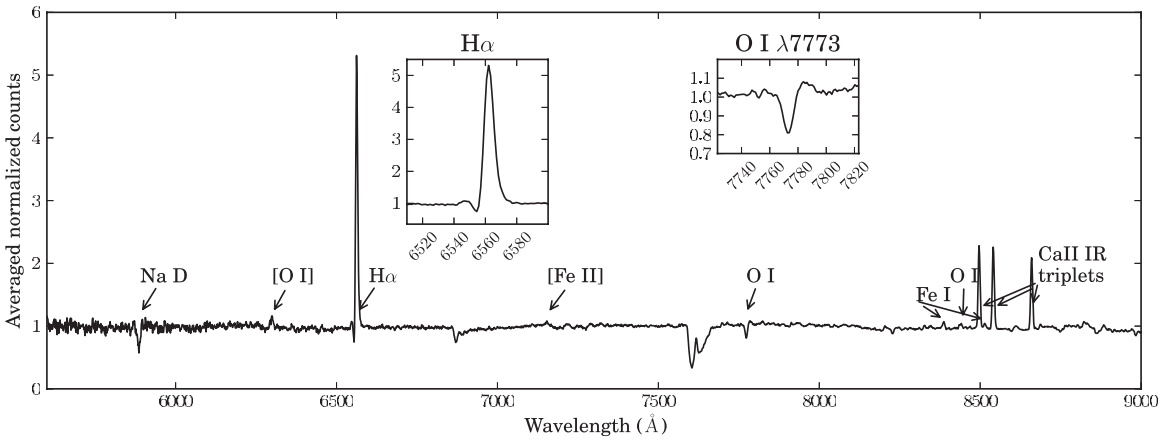

Figure 7. Spectral lines present in the spectrum of V1647 Ori are labeled above. To improve the signal-to-noise ratio, the normalized spectrum was obtained by weighted averaging of 33 HCT spectra taken over the outburst period 2008 September to 2013 March, each with an average exposure time of 40 minutes. The spectra are not corrected for atmospheric absorption lines. The absorption lines that are not labeled are atmospheric lines. Hα and O I λ7773 line profiles are shown more clearly in insets.

Table 4
Equivalent Widths (in Å) of Optical Lines in V1647 Ori

JD	Hα	Ca II λ8498	Ca II λ8542	Ca II λ8662	O I λ7773
2,454,724	−36.35	−8.601	−8.758	−8.125	2.483
2,454,725	−35.1	−8.686	−9.1	−7.678	1.754
2,454,743	−36.52	−12.97	−13.35	−12.19	1.491
2,454,744	−28.62	−10.75	−10.86	−10.12	2.407
2,454,755	−32.84	−7.61	−7.621	−7.819	1.839

Notes. Estimated error in equivalent widths of Hα lines is ∼±3 Å, error for Ca II IR triplet lines is ∼±0.5 Å, and the error for O I λ7773 lines is ∼±0.3 Å.
†† Observed from IGO; all other nights are from HCT.

(This table is available in its entirety in a machine-readable form in the online journal. A portion is shown here for guidance regarding its form and content.)

widths of Hα, Ca II IR triplet lines, and O I (7773 Å) are listed in Table 4.

3.3.1. Hα Line

The strong Hα line in V1647 Ori shows a clear P Cygni profile, as well as substantial variations. Figure 8 shows the variations of Hα profiles during our four and a half years of observations. P Cygni profiles were more prominent in the early part of the outburst in 2008. To see the absorption component clearly, a Gaussian is fitted to the right wing of the profile in red color and the difference of the fit to actual spectra is plotted in green color. Figure 9 shows the outflow velocity and associated error bar of expanding wind from the blueshifted absorption minima in the Hα profile. These blueshifted absorption components were present in the 2003 outburst also and disappeared during the fading stage of the outburst (Ojha et al. 2006; Fedele et al. 2007). Figure 10 shows the variation in equivalent width (W_λ in Å) of Hα emission. The calculation of W_λ was very sensitive to the weak continuum flux around 6563 Å, and the error estimate for each data point is $\sim \pm 3$ Å. The W_λ of the 2008 outburst is in a similar range as that during the first outburst in 2003. Since Hα emission comes from the innermost accretion-powered hot zone, we can expect its strength to be proportional to the accretion rate. The optical photometric magnitude in the second outburst is similar to that of the first outburst, which implies that the continuum flux is almost of the same value. Hence, from the fact that W_λ is of similar value as in the first outburst, we can deduce that the accretion rate is also of the same order in both outbursts during its "high plateau" stage.

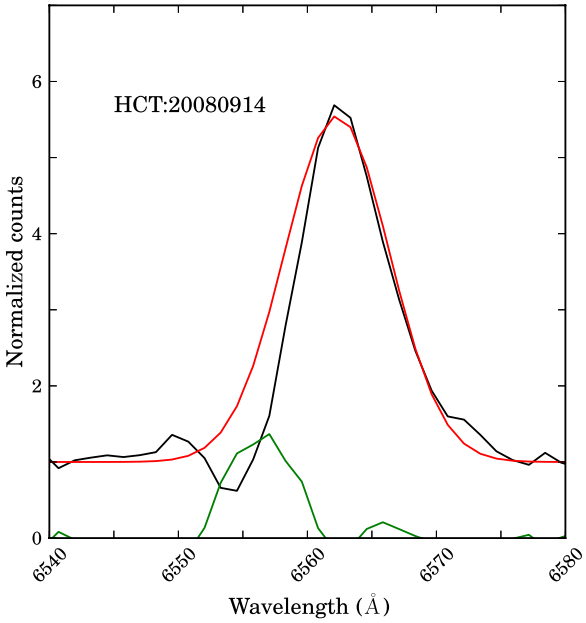

Figure 8. Variations of Hα profiles during our four-and-a-half-year observations. P Cygni profiles were more prominent in the early part of the outburst in 2008. A Gaussian is fitted to the right wing of the profile in red, and the difference of that Gaussian fit to actual spectra is plotted in green to show the absorption component clearly.

(A color version and the complete figure set (70 images) of this figure are available in the online journal.)

3.3.2. Ca II IR Triplet Lines

The plots of equivalent widths of Ca II IR triplet lines (8498, 8542, and 8662 Å) are shown in Figure 11. We have much lesser error bars (±0.5 Å) for the W_λ due to the higher continuum flux in these wavelengths. The Ca II IR triplet emission lines are seen to be in the ratio $1.07 \pm 0.09{:}1.15 \pm 0.1{:}1$. This nearly equal ratio is due to optically thick gas with the collision decay rates larger than the effective radiative decay rates of upper states of Ca II lines. Such an environment is typically seen in many T Tauri stars. Optical thickness, along with the non-detection of forbidden [Ca II] lines above noise, implies a number density of electrons of $\approx 10^{11}$ cm^{-3} (Hamann & Persson

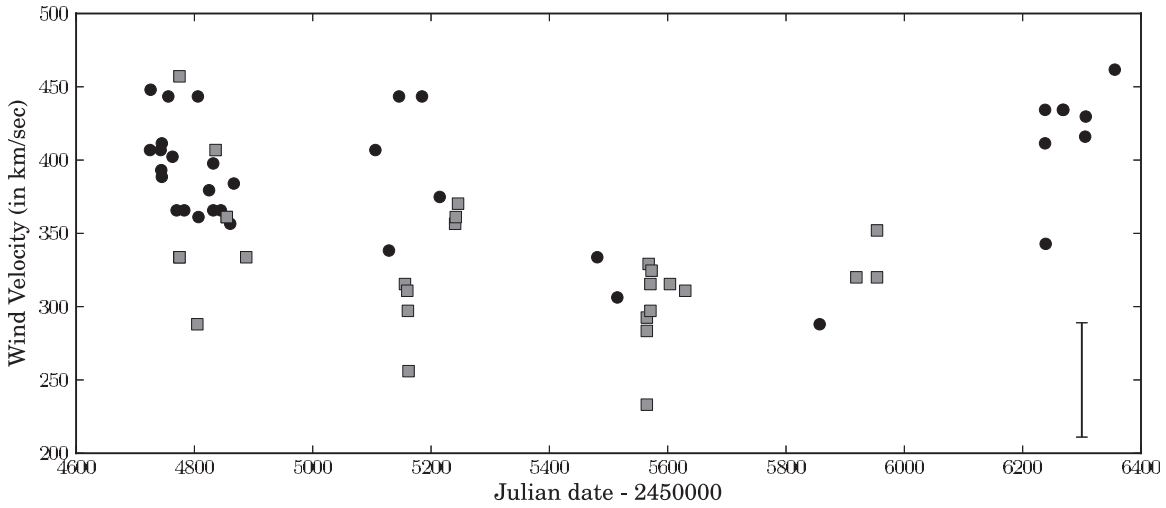

Figure 9. Velocity of expanding wind from the blueshifted absorption minima in the Hα P Cygni profile. The filled circles are from HCT, and gray filled squares are from IGO measurements. The error bar on the bottom right corner shows the typical ± 39 km s^{-1} error estimated for data points.

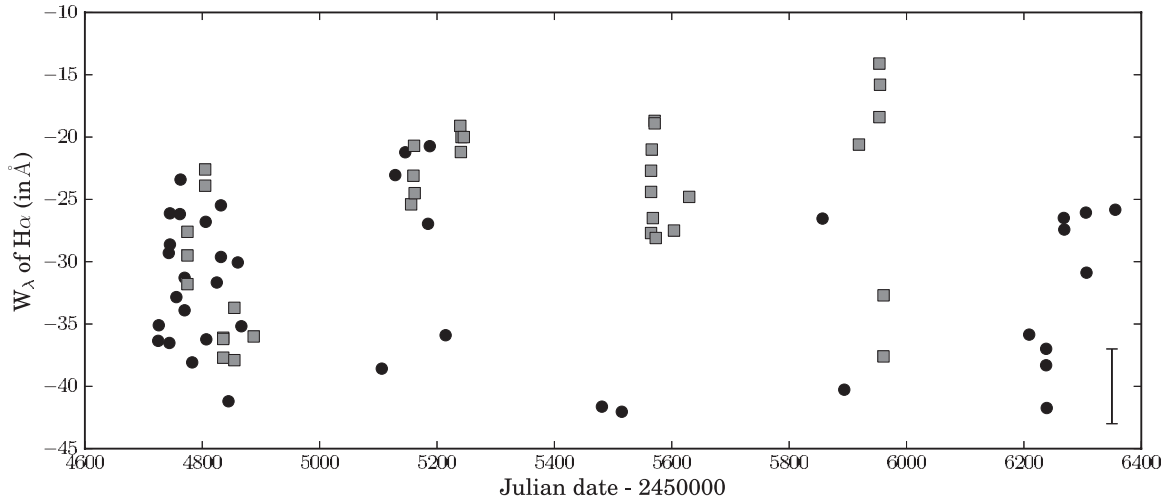

Figure 10. Variation in equivalent width of Hα emission. The filled circles are from HCT, and filled gray squares are from IGO measurements. Each data point has an error bar of $\sim\pm 3$ Å. This error bar is shown at the right bottom corner.

1992). For comparison with Figure 8 of Hamann & Persson (1992), Figure 12 shows the scatter plot between the ratios of equivalent widths, $W_{\lambda 8498}/W_{\lambda 8542}$ and $W_{\lambda 8662}/W_{\lambda 8542}$, of our data, as well as previously published data from literature. The error bar in our new data (black squares) is ± 0.1. From the position of the 2007 data point (red diamond) taken during quiescent phase (Aspin et al. 2008) in this scatter plot, Aspin et al. (2008, 2009) had concluded that the optical density of the region emitting Ca II IR triplet lines changed significantly between outburst and quiescent phases. But since there is only one data point from quiescent phase and it is lying within the scatter of points from the ongoing outburst, it might be difficult to conclude that the change in ratios observed was actually due to V1647 Ori moving from quiescent phase to outburst phase. We could see strong correlation between the equivalent widths (W_λ) of Ca II IR triplet lines (see Figure 13). The Pearson correlation coefficient (PCC) between both $W_{\lambda 8662}$ and $W_{\lambda 8498}$, and $W_{\lambda 8542}$ and $W_{\lambda 8498}$ is 0.88 with a two-tailed p value $\ll 0.0001$. This implies that the fluctuations in W_λ are not random statistical error. It could be due to fluctuations of continuum flux around 8500 Å. Peak-to-peak fluctuation of W_λ is ~ 5 Å, which means that if the flux from these lines is assumed to be constant, then the continuum flux has fluctuated by a factor of ~ 1.6, which in terms of the log scale of magnitude is ~ 0.5. This indeed matches with peak-to-peak fluctuation in I-band magnitude during the entire period. We do not see any strong correlation between W_λ of the Hα line and Ca II IR triplets. However, it should be noted that the error bars in W_λ of Hα are much higher than those of Ca II IR lines due to low continuum flux around 6563 Å.

In the 2008 October 29 spectrum, we could clearly detect the P Cygni profile in Ca II IR triplet lines (Figure 14). The strengths of the absorption trough of the three lines were in the same pattern as that of T Tauri star WL 22 (Hamann & Persson 1992), i.e., the pattern with strongest absorption in 8542 Å, then 8662 Å and very weak in 8498 Å. The ratio of W_λ of the blueshifted absorption between 8542 Å and 8662 Å is 0.76:0.45 = 1.69:1. This ratio is consistent within error bars with the 1.8:1 ratio of intensity from atomic transition strength of these lines. Hence, unlike the region producing emission lines, these absorption regions are optically thin. So by using the optically thin assumption, we can estimate the column density of Ca II by the formula (Spitzer 1978)

$$N_{\mathrm{Ca\,II}} = 1.1 \times 10^{20} \times \frac{\text{Å}}{\lambda}^2 \frac{1}{f_{\mathrm{lu}}} \frac{W_\lambda}{\text{Å}}\ \mathrm{cm}^{-2},$$

where the oscillator strength f_{lu} for the lines $\lambda\lambda 8542$ and 8662 are 0.39355 and 0.21478, respectively, taken from Merle

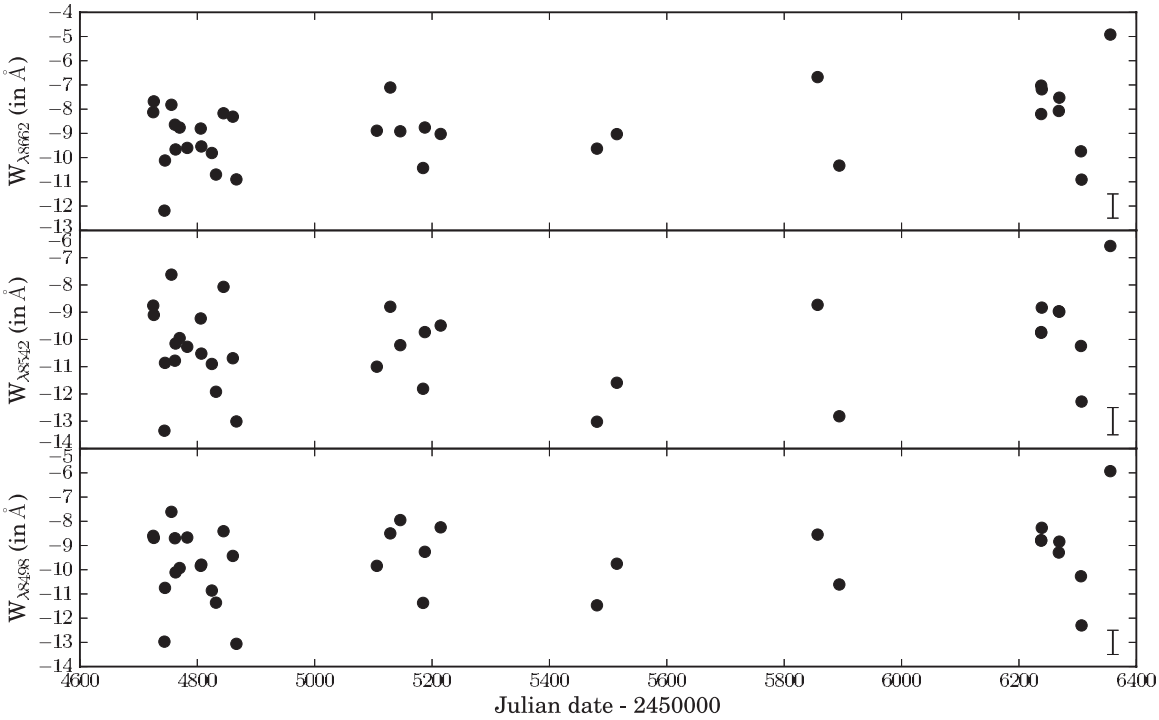

Figure 11. Variation in equivalent widths of Ca II IR triplet lines (λλ8498, 8542, and 8662) during the outburst period 2008 September to 2013 March. All data points are from HCT measurement, and each point has an error bar of ∼±0.5 Å. This error bar is shown at the right bottom corner. Due to limited spectral range in the IGO grism, Ca II triplet lines were not observed from IGO.

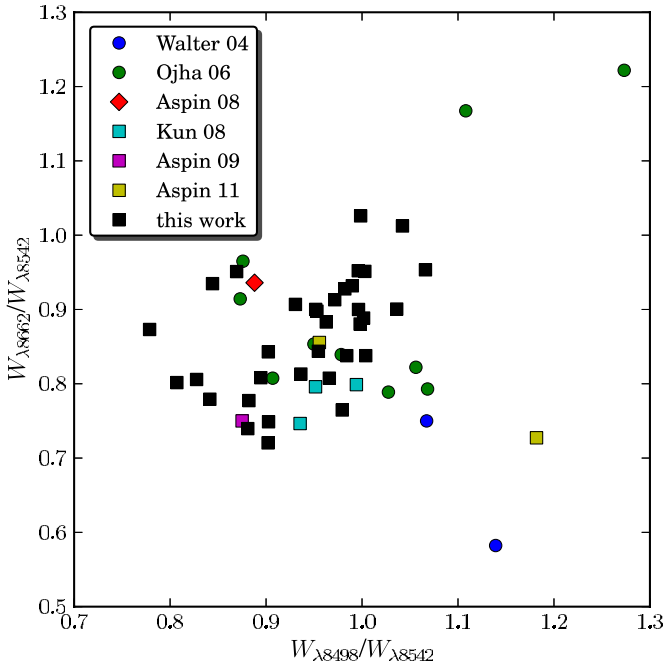

Figure 12. Ratio of Ca II IR triplet lines' equivalent widths, $W_{\lambda8498}/W_{\lambda8542}$ vs. $W_{\lambda8662}/W_{\lambda8542}$, of our data, as well as previously published data from the literature. 2003 outburst points are shown as circles (Walter et al. 2004; Ojha et al. 2006), 2008 outburst points are shown as squares (Kun 2008; Aspin et al. 2009; Aspin 2011; this work), and the 2007 quiescent phase point is shown as a diamond (Aspin et al. 2008). The typical error bar on our new data (black squares) is ∼±0.1.

(A color version of this figure is available in the online journal.)

et al. (2011). Substituting the W_λ, wavelength and oscillator strength for both lines, we get the column density ($N_{\mathrm{Ca\,II}}$) as 2.9×10^{12} cm^{-2} and 3×10^{12} cm^{-2}, respectively. This is the column density of Ca II atoms in this small duration of outflow wind. Assuming reasonable estimates of temperature $T = 2600$ K (disk temperature estimated by Rettig et al. 2005) and pressure $P = 1$ Pascal (typical pressure in solar winds), the fraction of ionization using Saha's formula is ≈0.004. Hence, dividing by this fraction, we obtain the column density of Ca atoms in the gas blob to be $\approx 7.5 \times 10^{14}$ cm^{-2}. Assuming solar metallicity, we obtained the column density of hydrogen (H) in the outflowing gas blob as $\approx 3.4 \times 10^{20}$ cm^{-2}. From the Doppler shift of the absorption minima, we also obtained a wind velocity of 313 ± 10 km s^{-1} (in the λ8542 line) and 303 ± 10 km s^{-1} (in the λ8662 line). We also detected a faint P Cygni profile in the λ8542 line on 2008 December 30, with a blueshifted velocity of 329 ± 10 km s^{-1}. Apart from these two episodic events, none of our other spectra show any detectable P Cygni profile. The episodic nature of these two winds implies they are magnetic reconnection driven winds rather than pressure driven steady winds.

Even though our medium-resolution spectra cannot be used to study line widths, since the Ca II IR triplets are nearby, we could do relative comparison of the widths of the Ca II IR triplet lines, where width is taken to be the FWHM of the Gaussian fit of the continuum normalized profile. Since this quantity is the FWHM of the Gaussian profile that we get after the convolution of instrument response on the actual line, it is not the FWHM of the line. However, since the lines are very close and the instrumental convolution is common, the wider line will give a wider FWHM after convolution. Figure 15 shows a scatter plot of the ratio of the widths of λ8498 and λ8542 versus the equivalent width of the line λ8542. Most of the points lie below 1.0 in the ratio axis. Using the "test statistic" for mean with 34 data points, we could reject null hypothesis *H_0: the mean of the ratio is 1*, with 6σ confidence. This shows that the λ8498 line is slightly narrower than the λ8542 line. A similar

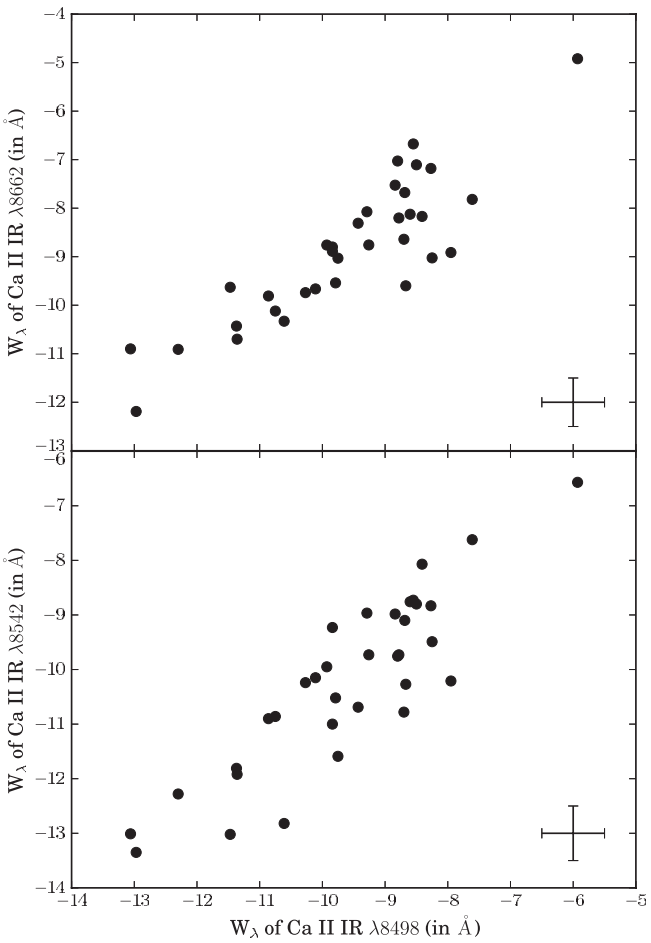

Figure 13. Strong correlation between the equivalent widths of Ca II IR triplet lines. Typical error bar is given at the right bottom corner. The Pearson correlation coefficient (PCC) between both $W_{\lambda 8662}$ and $W_{\lambda 8498}$ and $W_{\lambda 8542}$ and $W_{\lambda 8498}$ is 0.88 with a two-tailed p value $\ll 0.0001$.

trend is seen in most of the T Tauri stars (Hamann & Persson 1992). Apart from showing this skewness, since our spectra are of only medium resolution, we cannot quantify the narrowness of the line. This narrowness of the optically thinner line λ8498 could be explained by either substantial opacity broadening in λ8542 (since 1:9 is the ratio of atomic line strength) or lower dispersion velocity in the inner part of the region of Ca II IR emission (Hamann & Persson 1992).

Our period search in the equivalent width (W_λ) of Ca II IR triplet lines found six faint periodicities in all three lines in the range of 1–100 days with $\sim 2\sigma$ confidence level in amplitude. The possible periodicities and confidence were estimated by the Lomb–Scargle periodogram along with Monte Carlo simulation. The possible periods are 3.39, 8.09, 27.94, 30.8, 40.77, and 45.81 days. Since the amplitudes are only of 2σ confidence level, they can be confirmed only with more observations. Figure set 16 shows the folded data of the entire four-and-a-half-year observations and the statistical significance of the amplitudes. The amplitude of the least-squares fitted cosine function is ∼1. If this periodicity is due to change in the continuum flux, the corresponding amplitude of magnitude change we expect in logarithmic I-band magnitude is ∼0.1. This is not much above our error in magnitude estimate, so the fact that we do not see similar periodicity in I-band magnitude does not rule out the cause of change in W_λ as change in continuum flux. We also do not see any corresponding significant periodicity in W_λ of Hα.

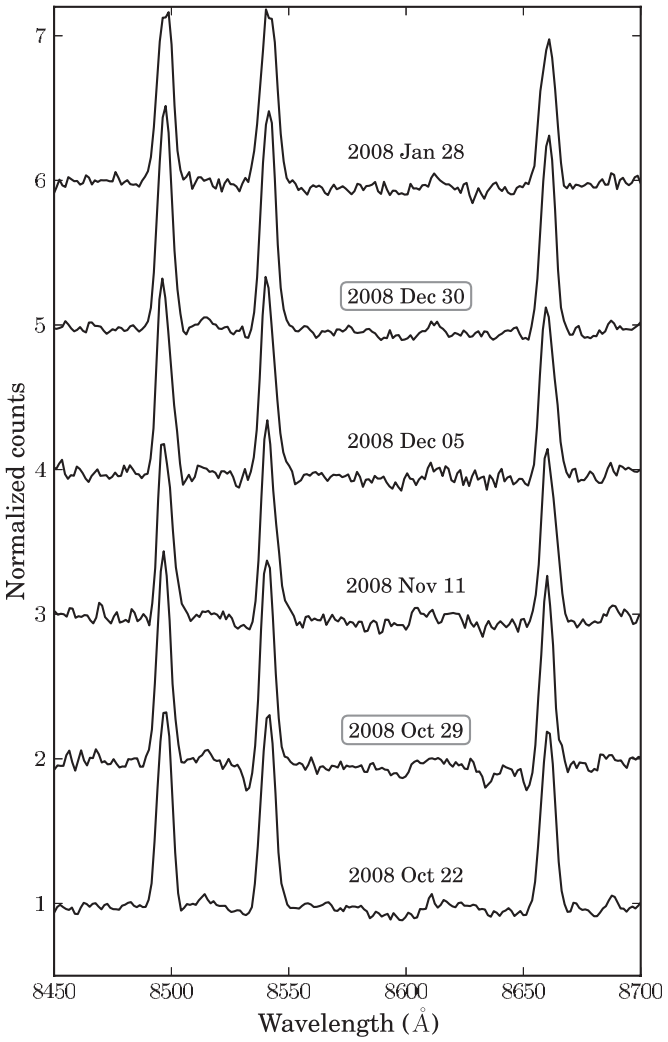

Figure 14. Spectrum of V1647 Ori taken on 2008 October 29 showing a clear P Cygni profile in Ca II IR triplet lines. A similar but fainter profile was once more detected in 2008 December 30. None of the other nights' spectra showed this profile. For comparison, available nearby nights' spectra are also plotted.

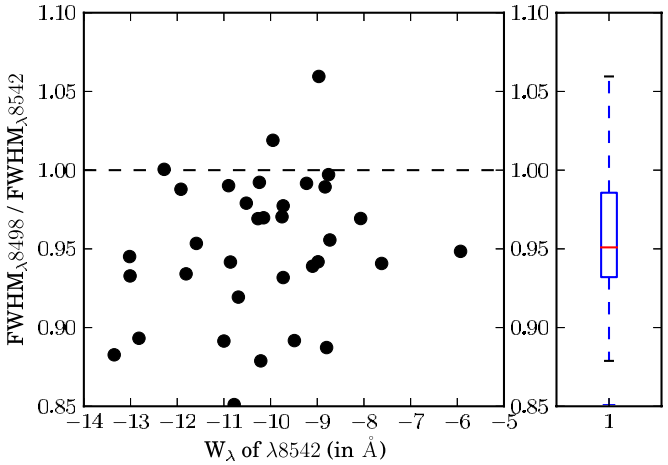

Figure 15. Scatter plot of the ratio of the widths of λ8498 and λ8542 vs. equivalent width of the line λ8542. Most of the points lie below 1.0 in the Y-axis. A box and whisker plot of the distribution is also plotted on the right side. This shows that the λ8498 line is slightly narrower than the λ8542 line.
(A color version of this figure is available in the online journal.)

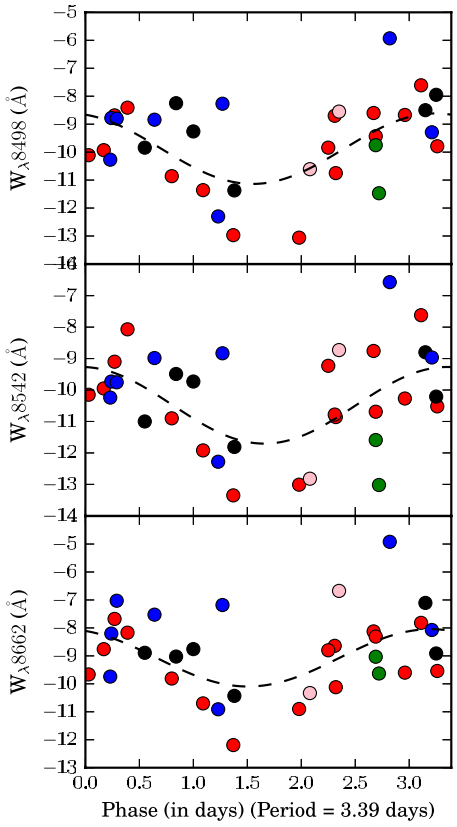

Figure 16. Folded phase plot of the W_λ of Ca II IR triplet lines λ8498, λ8542, and λ8662 (in Å), and *I*-band magnitude. The folding is done over the entire four and a half years of data. The red, black, green, pink, and blue circles correspond to data of 2008, 2009, 2010, 2011, and 2012 winter observations, respectively. The amplitudes (in Å) of the three lines in each folded plot are as follows. For a period of 3.39 days: 1.26 ± 0.69, 1.22 ± 0.75, 1.03 ± 0.67; for a period of 8.09 days: 1.13 ± 0.70, 1.33 ± 0.71, 1.17 ± 0.65; for a period of 27.94 days: 1.13 ± 0.72, 1.11 ± 0.79, 1.14 ± 0.67; for a period of 30.8 days: 1.26 ± 0.61, 1.25 ± 0.63, 0.98 ± 0.58; for a period of 40.77 days: 1.26 ± 0.65, 1.42 ± 0.58, 1.18 ± 0.59; for a period of 45.81 days: 0.95 ± 0.76, 1.29 ± 0.74, 1.10 ± 0.68.

(An extended, color version of this figure is available in the online journal.)

Aspin et al. (2008) took the spectrum of V1647 Ori during the quiescent phase in 2007 February. The W_λ of both Ca II IR triplet lines and Hα were ∼3.3 times the present value. Aspin & Reipurth (2009) had used the ratio of W_λ of Hα between the 2003 outburst and quiescent phase to estimate change in accretion rate. Similarly, since the continuum flux changed by a factor of ∼40 between the quiescent and 2008 outburst phase, we can estimate that the change in the line flux of both sets of lines is by a factor of ∼10. This agrees with the change in accretion rate. Thus, the origin of Ca II IR triplet lines is directly connected to the accretion rate just like Hα. This is in agreement with the finding of tight correlation between Ca II IR line flux and accretion rate in T Tauri stars by Muzerolle et al. (1998), which suggests that the origin of these lines is in the magnetospheric infall zone. The similar value of W_λ of Ca II IR lines with that of 2003 also strengthens the claim that the accretion rate onto the star from the inner disk was the same during both outbursts.

3.3.3. Oxygen Lines

The most prominent oxygen line is O I λ7773 in absorption; however, weak O I λ8446 line is also detected in emission. We should be careful in interpreting the W_λ of the O I λ7773 absorption line because the profile shape of the line seems to be a combination of the redshifted emission component and more stronger blueshifted absorption component (see Figure 7). A weak anti-correlation is seen between Hα and O I λ7773 (see Figure 17). Correlation had PCC = 0.54, with a two-tailed p value of 0.001. This anti-correlation in W_λ of O I λ7773 and Hα could be due to positive correlation between emission component of O I λ7773 filling in the absorption dip and Hα. Since O I λ7773 cannot be formed in the photosphere of cool stars, the absorption component is due to warm gas in the envelope or hot photosphere above the disk, while the emission component might be due to the hot gas region from which Hα is also being emitted. Ojha et al. (2006) reported a decreasing trend in the W_λ of O I λ7773 from the beginning until the end of the 2003 outburst, which was interpreted to be a possible decrease in turbulence in the outer envelope during the outburst period. We do not see such a trend in the 2008 outburst, but the values of W_λ in the 2008 outburst remain the same as that during the second half of the 2003 outburst. A slight decrease of W_λ in the later part of the 2003 outburst observed on 2005 September 8, as reported by Ojha et al. (2006), in contrast to the increase of W_λ of other lines, could be due to an increase in the W_λ of the O I λ7773 emission component.

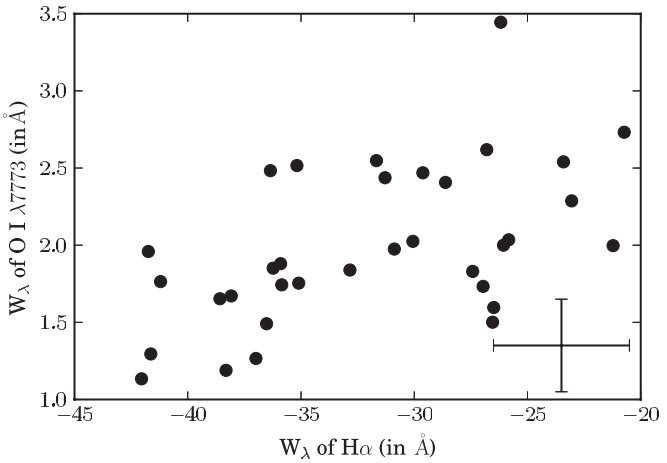

Figure 17. Correlation between equivalent width of Hα and O I λ7773. Typical error bar is given at the right bottom corner. PCC is 0.54 with a two-tailed p value of 0.001. The weak anti-correlation could be due to a positive correlation between the Hα and redshifted emission component that is filling the absorption component in the O I λ7773 profile. Bootstrap analysis gave a 95% confidence range of PCC of [0.29, 0.72].

3.3.4. Forbidden Lines

We detected [O I] (6300 Å) and [Fe II] (7155 Å) forbidden line emissions in V1647 Ori's spectra. The presence of [O I] λ6300 and [Fe II] λ7155 implies shock regions probably originating from jets. This, combined with non-detection of the [S II] (6731 Å) line above our noise level, implies that the shock region has temperature $T \approx$ 9000–11,000 K and electron number density $\approx 10^5$–10^6 cm^{-3} (Hamann 1994). We see significant variations in the strengths of the forbidden lines [O I] and [Fe II]; however, the lines are too faint in our individual spectra to quantify statistically. During the fading stage of the 2003 outburst in 2006 January, when the bright continuum flux decreased, Fedele et al. (2007) were also able to detect various strong forbidden line emissions, namely, [O I] λλ6300, 6363, [S II] λλ6717, 6731, and [Fe II] λ7172.

4. IMPLICATION ON MODELS OF OUTBURST

The models that are known for FUor/EXor outbursts can be broadly classified into three types. The first kind of model is

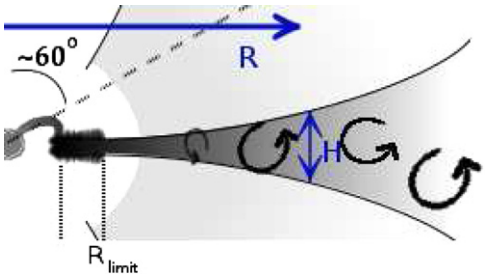

Figure 18. Cross section of an α disk. R is the radial distance from the star, and H is the thickness of the disk, which flares up as the radius R increases. $R_{\rm limit}$ is the radius up to which the outburst extends. We are looking into the system at ~60° along the dashed line drawn in the figure. In the α disk model, the viscosity is due to large turbulent eddies. The speed of eddies is upper bounded by the velocity of sound (c_s) because any supersonic flow will get dissipated by shock. The size of eddies is also upper bounded by the thickness (H) of the disk. Thus, taking α to be a free parameter <1, we get the viscosity in the disk as $\nu = \alpha c_s H$. The orbital velocity is taken to be Keplerian in our problem.

(A color version of this figure is available in the online journal.)

purely a thermal instability model, initially proposed for dwarf nova systems and was later adapted for the FUors kind of outbursts (Bell & Lin 1994). The second kind of model involves a binary companion or planet, which perturbs the disk, causing repeated sudden high-accretion events (Bonnell & Bastien 1992; Lodato & Clarke 2004). The third kind involves mainly gravitational instability (GI) triggering magnetorotational instability (MRI; Zhu et al. 2009, and references therein). The Bell & Lin (1994) model (hereafter BL94) is a pure thermal instability model. In BL94, the thermal instability is triggered when the surface density at a region in the disk rises above a critical density. The viscous timescales determine duration of outbursts and quiescent phase. The inner region at a radius r during outburst will deplete below the critical surface density in viscous timescale $\tau_{\rm visc} = r^2/\nu$. Based on α prescription of viscosity, $\nu = \alpha c_s H$, where c_s is the isothermal sound speed, $H \approx c_s/\Omega$ is the disk thickness, Ω is orbital angular velocity at radius r, and α (< 1) is a dimensionless parameter (see Figure 18). Substituting, we get the relation

$$\tau_{\rm visc} = \frac{r^2\Omega}{\alpha c_s^2} = \frac{1}{\alpha\Omega}\left(\frac{r}{H}\right)^2.$$

Let $v_R \approx r/\tau_{\rm visc} \approx \nu/r$ be the effective inward radial velocity component of gas in the inner accretion disk. Then the mass infall rate at radius R is $\dot{M} = -2\pi R\Sigma v_R$, where Σ is the surface density of the disk at that radius. Substituting v_R, ν, and H in the above equation of $\dot{M}$, we get $\dot{M} \approx 2\pi\Sigma\alpha c_s^2/\Omega$. The timescale of transition between outburst and quiescent phases is much smaller than the viscous timescale. Hence, Σ will remain constant, and Ω will also remain constant at a given R, which leaves only the parameter αc_s^2 to explain the change by a factor of ~10 in inner disk accretion rate to V1647 Ori between the outburst and quiescent phases. Since the square of isothermal sound speed $c_s^2 = R_g T/\mu$ (where R_g is the gas constant, T is temperature, and μ is mean molecular weight), the temperature change by a factor of 10 between the phases at the trigger of thermal instability (Zhu et al. 2009, Appendix B, their Figure 14) alone will cause a net change in accretion rate by a factor of 10. Hence, at least in the inner region of the disk, α can change only by a multiplicative factor of order 1 to remain consistent with the observed change in accretion rate.

In BL94, assuming the mass infall rate to the inner disk region $\dot{M}_{\rm in}$ = constant, the α determines the timescales and the ratio $\alpha_{\rm outburst}/\alpha_{\rm quiescent}$ is proportional to the ratio of time in quiescent phase to time in outburst phase (BL94; Table 2). Figure 19 shows the schematic of the light curve of V1647 Ori in optical band that we know so far. The photometric magnitudes and overall SED during the quiescent phase in 2007 match with pre-2003 outburst data (Aspin et al. 2008). Even though accretion rate had fallen by a factor of 10 during quiescent phase, it was still on the order of $10^{-6}\ M_\odot\ {\rm yr}^{-1}$. Based on this, Aspin et al. (2009) had suggested that the 2003 outburst might not have actually terminated in 2006. Since we do not have a good estimate of the pre-outburst accretion rate, we shall consider this sudden drop in accretion rate by a factor of 10 as a drop from outburst state to quiescent phase in outburst models.

Let α_{o1}, α_{o2}, and α_{o3} represent the three outburst phase α values and α_{q1} and α_{q2} represent the two quiescent phase α values. If we assume $\dot{M}_{\rm in}$ = constant in BL94, from the ratio of periods, we get the following relations: $\alpha_{o1} = k(22\text{–}89)\alpha_{q1}$, $\alpha_{o2} = k21\alpha_{q1}$, $\alpha_{o3} < k9\alpha_{q1}$, $\alpha_{o3} < k0.6\alpha_{q2}$, where k is just the proportionality constant corresponding to the constant $\dot{M}_{\rm in}$. We also get $\alpha_{o2} = (0.23\text{–}0.95)\alpha_{o1}$, $\alpha_{o3} < 0.4\alpha_{o2}$, $\alpha_{q2} = 15\alpha_{q1}$. This is a very huge variation in α parameter. However, our accretion estimates, during the 2003 as well as 2008 outbursts, show that the accretion rate of matter onto the star from the inner disk was quite stable at ~10 times the rate in quiescent phase. Thus, the α parameter cannot be fluctuating as much as we estimated; especially $\alpha_{o3} < k0.6\alpha_{q2}$ is impossible from the fact that viscosity has to be more in outburst phase than quiescent phase. Then the assumption $\dot{M}_{\rm in}$ = constant in BL94 might be wrong. An increase in $\dot{M}_{\rm in}$ can decrease the draining rate of the inner disk and can account for a longer duration of the outburst period. It can also explain the slower rate of dimming in the magnitude of the V1647 Ori during its plateau stage in the present outburst compared to the 2003 outburst.

By letting $\dot{M}_{\rm in}$ be a variable and substituting $R_{\rm limit}$ to be the radius up to which instability extends, to constrain parameters, we compared the viscous timescale $\tau_{\rm visc} = R_{\rm limit}^2/\nu \approx R_{\rm limit}^2\Omega/\alpha c_s^2$ between the 2003 and 2008 outbursts. The instability triggering temperature at the boundary has to be the same for both

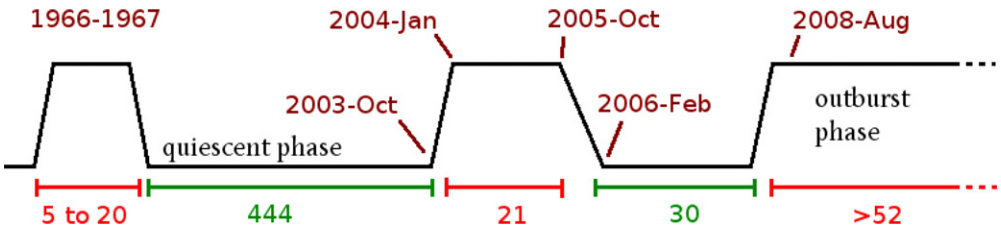

Figure 19. Optical light-curve history of V1647 Ori. The duration of each outburst and quiescent period is marked in units of months. The X-axis of the image is not drawn to scale.

(A color version of this figure is available in the online journal.)

outbursts, so the sound speed c_s will be the same. Parameter α can also be taken to be the same during both outbursts based on our previous conclusion. Now the only free variable parameter that determines the timescale is $R_{\rm limit}$. Substituting Keplerian $\Omega \propto R^{-(3/2)}$, we finally obtain the relation for viscous timescale in terms of $R_{\rm limit}$ to be $\tau_{\rm visc} \propto R_{\rm limit}^{1/2}$.

BL94 gives the radius up to which instability extends to

$$R_{\rm limit} = 20\, R_\odot \left(\frac{\dot{M}_{\rm in}}{3\times10^{-6}\, M_\odot\ {\rm yr}^{-1}}\right)^{\frac{1}{3}} \left(\frac{M_*}{M_\odot}\right)^{\frac{1}{3}} \left(\frac{T_{\rm eff}}{2000}\right)^{-\frac{4}{3}} \propto \dot{M}_{\rm in}^{\frac{1}{3}}.$$

Substituting this proportionality, we get $\tau_{\rm visc} \propto \dot{M}_{\rm in}^{(1/6)}$. Thus, the ratios of mass infall rate from outer to inner disk during each outburst are related to the duration of outburst by the relation $(\dot{M}_{\rm in_{2008}}/\dot{M}_{\rm in_{2003}}) > (52/21)^6 \approx 230$. Thus, the infall of gas from outer to inner disk during the 2008 outburst is at least 230 times (two orders) more than that during the 2003 outburst.

The model presented by Zhu et al. (2010) includes an MRI instability contribution to viscosity parameter if the temperature of the disk goes above the MRI triggering temperature (T_M) and also includes an effective viscosity contribution from GI beyond the radius given by Toomre's instability parameter Q. The relation between $R_{\rm limit}$ and $\dot{M}$ in this model is $R_{\rm limit} \propto \dot{M}^{(2/9)}$. Thus, $\tau_{\rm visc} \propto \dot{M}_{\rm in}^{(1/9)}$, and hence $(\dot{M}_{\rm in_{2008}}/\dot{M}_{\rm in_{2003}}) > (52/21)^9 \approx 3500$. Therefore, the infall of gas from outer to inner disk during the 2008 outburst is at least 3500 times (three orders) more than that during the 2003 outburst. This estimate is one order more than BL94. It should be kept in mind that the viscosity timescale gives only an order-of-magnitude estimate of the duration of outburst. For a comparison of actual simulated duration of outburst and viscous timescale see Table 1 in Zhu et al. (2010). If the present outburst continues for a larger period, $\dot{M}_{\rm in_{2008}}/\dot{M}_{\rm in_{2003}}$ will further increase. Since we have an upper limit in $\dot{M}_{\rm in}$ for FUors, the increased ratio could only be explained as a dip in mass inflow in 2003. For example, a gap in the disk could have resulted in the sudden ending of the 2003 outburst. This gap or low-density region has to be near the typical $R_{\rm limit}$ predicted by each model, i.e., ~1 AU.

To estimate the change in photometric magnitudes between 2003 and 2008 outburst phase due to predicted change in radius $R_{\rm limit}$, we modeled a disk with temperature profile given by outburst accretion rate inside $R_{\rm limit}$ and quiescent accretion rate outside $R_{\rm limit}$. The magnitude variations in optical I and NIR J bands were found to be less than 1 mag for variation of $R_{\rm limit}$ by a factor of six. Mosoni et al. (2013) reported an increase in visibility of the resolved interferometric study of V1647 Ori using VLTI/MIDI observations in the 8–13 μm range during the early stage of fading in the 2003 outburst (between 2005 March and 2005 September). Apart from the possible scenarios discussed by Mosoni et al. (2013), it could also be explained by the relative increase in contribution in total flux from the extended outburst disk when the central star's accretion slowed down. A similar VLTI/MIDI visibility study of the ongoing 2008 outburst will give more input to constrain $R_{\rm limit}$ and outburst models.

Thus, we conclude that a pure thermal instability alone cannot explain the varying timescales of outbursts occurring in V1647 Ori. As proposed for other short rise timescale FUors, V1647 Ori can also be explained only by an outside-in triggering of the instability from outer radius (Bell & Lin 1994). The change in inflow of material from outer to inner disk could be due to many possibilities like MRI, GI, or planet perturbation. The smooth surface density assumptions of the disk also might not be a good model in light of detection of a clump in the disk at 0.27 AU and disappearance of it in the second outburst.

Our observations detected a variety of episodic events like sudden short-duration winds with hydrogen column density $\approx 3.4 \times 10^{20}$ cm^{-2}, fluctuations in Hα flux, short timescale variation in continuum flux, etc. The short timescale variation in continuum flux could be explained by the convections in the inner disk as suggested by Zhu et al. (2009) for their model of the FU Orionis disk. The variations in Hα flux could have their origin in some magnetic phenomena in the accretion funnel. The episodic wind events, [Fe II] λ7155, and [O I] λ6300 could be originating from jets or the disk/stellar wind region. If we compare between 2008 and 2003 outbursts, the accretion rate onto the star from the inner disk, extinction in NIR CC diagram, outburst magnitude, and spectral signatures in optical are the same. The main difference between 2008 compared to 2003 is the larger duration of outburst phase, six times slower dimming rate in optical during its "plateau" stage, and the change in circumstellar gas distribution revealed by morphological change in the nebula's illumination.

5. CONCLUSIONS

We have carried out four and a half years of continuous monitoring of V1647 Ori in its second outburst phase starting from 2008. Following are our main conclusions.

1. V1647 Ori is still in outburst "plateau" stage, at similar magnitude to the 2003 outburst in optical and NIR bands. It is undergoing a slow dimming at a rate of 0.04 mag yr^{-1}, which is six times slower than the rate during the 2003 outburst. The magnitude shows significant short-timescale (~1 day) variations.
2. Morphological studies on illumination of the nebula show a consistent change in the circumstellar gas distribution between 2008, 2003, and 1966 outbursts.
3. P Cygni profiles in Hα emission lines show outflowing wind velocities of ~350 km s^{-1}. Apart from the continuous wind, we also detected twice short-duration episodic winds driven by magnetic reconnection events, with H column density $\approx 3.4 \times 10^{20}$ cm^{-2} from P Cygni profiles in Ca II IR triplet lines in 2008 October and December. From Ca II IR triplet and Hα line strengths, the accretion rate was found to be the same as that during the 2003 outburst and is ~10 times more than the quiescent phase.
4. We could not detect the 56 day periodicity seen in the 2003 outburst.
5. Detection of the forbidden [O I] λ6300 and [Fe II] λ7155 lines implies shock regions of $T \approx$ 9000–11,000 K and $n_e \approx 10^5$–10^6 cm^{-3}, probably originating from jets.
6. Timescales of outburst history of V1647 Ori cannot be explained by a simple thermal instability model by Bell & Lin (1994) alone. To explain the large change in accretion rate from outer to inner disk between the last two outbursts, we require more comprehensive models that include contribution from MRI, GI, and planetary perturbations. From the framework of instability models we conclude that the sudden ending of the 2003 outburst could be due to a gap or low-density region in the inner (~1 AU) disk.

We thank the anonymous referee for giving us invaluable comments and suggestions that improved the content of the paper. The authors thank the staff of HCT, operated by Indian Institute of Astrophysics, Bangalore, and IGO at Girawali, operated by Inter-University Centre for Astronomy and Astrophysics, Pune, for their assistance and support during observations. It is a pleasure to thank J. S. Joshi and all the members of the Infrared Astronomy Group of TIFR for their support during the TIRCAM2 campaign. All the plots were generated using the two-dimensional graphics environment *Matplotlib* (Hunter 2007).

REFERENCES

Ábrahám, P., Mosoni, L., Henning, T., et al. 2006, A&A, 449, 13
Acosta-Pulido, J. A., Kun, M., Ábrahám, P., et al. 2007, AJ, 133, 2020
Andrews, S. M., Rothberg, B., & Simon, T. 2004, ApJL, 610, L45
Aspin, C. 2011, AJ, 142, 135
Aspin, C., Barbieri, C., Boschi, F., et al. 2006, AJ, 132, 1298
Aspin, C., Beck, T. L., & Reipurth, B. 2008, AJ, 135, 423
Aspin, C., & Reipurth, B. 2009, AJ, 138, 1137
Aspin, C., Reipurth, B., Beck, T. L., et al. 2009, ApJL, 692, L67
Bell, K. R., & Lin, D. N. C. 1994, ApJ, 427, 987
Bessell, M. S., & Brett, J. M. 1988, PASP, 100, 1134
Bonnell, I., & Bastien, P. 1992, ApJ, 401, 654
Briceño, C., Vivas, A. K., Hernández, J., et al. 2004, ApJL, 606, L123
Evans, N. J., II, Dunham, M. M., Jørgensen, J. K., et al. 2009, ApJS, 181, 321
Fedele, D., Van den Ancker, M. E., Petr-Gotzens, M. G., & Rafanelli, P. 2007, A&A, 472, 207
Hamaguchi, K., Grosso, N., Kastner, J. H., et al. 2012, ApJ, 754, 32
Hamann, F. 1994, ApJS, 93, 485
Hamann, F., & Persson, S. E. 1992, ApJS, 82, 247
Hartmann, L. 1998, Accretion Processes in Star Formation (Cambridge: Cambridge Univ. Press)
Hartmann, L., & Kenyon, S. J. 1996, ARA&A, 34, 207
Herbig, G. H. 1977, ApJ, 217, 693
Hunt, L. K., Mannucci, F., Testi, L., et al. 1998, AJ, 115, 2594
Hunter, J. D. 2007, CSE, 9, 90
Ioannidis, G., & Froebrich, D. 2012, MNRAS, 425, 1380
Kastner, J. H., Richmond, M., Grosso, N., et al. 2004, Natur, 430, 429
Kenyon, S. J., Hartmann, L. W., Strom, K. M., & Strom, S. E. 1990, AJ, 99, 869
Kóspál, A., Ábrahám, P., Acosta-Pulido, J., et al. 2005, IBVS, 5661, 1
Kun, M. 2008, IBVS, 5850, 1
Landolt, A. U. 1992, AJ, 104, 340
Lodato, G., & Clarke, C. J. 2004, MNRAS, 353, 841
McNeil, J. W. 2004, IAUC, 8284, 1
Merle, T., Thévenin, F., Pichon, B., & Bigot, L. 2011, MNRAS, 418, 863
Meyer, M. R., Calvet, N., & Hillenbrand, L. A. 1997, AJ, 114, 288
Mosoni, L., Sipos, N., Ábrahám, P., et al. 2013, A&A, 552, A62
Muzerolle, J., Hartmann, L., & Calvet, N. 1998, AJ, 116, 455
Naik, M. B., Ojha, D. K., Ghosh, S. K., et al. 2012, BASI, 40, 531
Ninan, J. P., Ojha, D. K., Mallick, K. K., et al. 2012, CBET, 3164, 1
Ojha, D. K., Ghosh, S. K., Tej, A., et al. 2006, MNRAS, 368, 825
Ojha, D. K., Kusakabe, N., Tamura, M., et al. 2005, PASJ, 57, 203
Pringle, J. E. 1981, ARA&A, 19, 137
Reipurth, B., & Aspin, C. 2004, ApJL, 606, L119
Rettig, T. W., Brittain, S. D., Gibb, E. L., Simon, T., & Kulesa, C. 2005, ApJ, 626, 245
Rieke, G. H., & Lebofsky, M. J. 1985, ApJ, 288, 618
Scholz, A., Froebrich, D., & Wood, K. 2013, MNRAS, 430, 2910
Spitzer, L., Jr. 1978, Physical Processes in the Interstellar Medium (New York: Wiley)
Teets, W. K., Weintraub, D. A., Grosso, N., et al. 2011, ApJ, 741, 83
Vacca, W. D., Cushing, M. C., & Simon, T. 2004, ApJL, 609, L29
Venkata Raman, V., Anandarao, B. G., Janardhan, P., & Pandey, R. 2013, RAA, 13, 1107
Vig, S., Ghosh, S. K., Kulkarni, V. K., & Ojha, D. K. 2006, A&A, 446, 1021
Walter, F. M., Stringfellow, G. S., Sherry, W. H., & Field-Pollatou, A. 2004, AJ, 128, 1872
Zhu, Z., Hartmann, L., Gammie, C., & McKinney, J. C. 2009, ApJ, 701, 620
Zhu, Z., Hartmann, L., Gammie, C. F., et al. 2010, ApJ, 713, 1134